

# Illumination-Driven Energy Level Realignment at Buried Interfaces between Organic Charge Transport Layers and a Lead Halide Perovskite

Fengshuo Zu, Marcel Roß, Lennart Frohloff, Dongguen Shin, Nir Tessler, Steve Albrecht, and Norbert Koch\*

Tremendous progress in employing metal halide perovskites (MHPs) in a variety of applications, especially in photovoltaics, has been made in the past decade. To unlock the full potential of MHP materials in optoelectronic devices, an improved understanding of the electronic energy level alignment at perovskite-based interfaces is required. This particularly pertains to such interfaces under device operation conditions, e.g. under illumination with visible light such as in a solar cell. Herein, it is revealed that the energy level alignment at the buried interface between a double cation lead halide perovskite film and charge-selective organic transport layers changes upon white light illumination. This is found from photoemission experiments performed with the samples in dark and under illumination, and the interfacial energy level shift is reversible. The underlying mechanism is attributed to the accumulation of one charge carrier type within the perovskite film at the interface under illumination, as a result of the charge-selective nature of the organic layer. The fact that the interfacial energy level alignment at MHP-based junctions under illumination can differ from that in dark is to be taken into account to fully rationalize device characteristics.

## 1. Introduction

In the past decade, metal halide perovskites (MHPs), owing to their outstanding optoelectronic properties, have enabled remarkable progress in a variety of applications.<sup>[1–4]</sup> In particular, MHP-based photovoltaics has exhibited an unprecedented rate of increase in power conversion efficiency,<sup>[5–7]</sup> which has already surpassed the conventional thin-film technologies on the level of laboratory research.<sup>[5]</sup> To continue boosting the performance of MHP-based solar cells, further reduction of the energy losses in devices is needed to exploit the full potential of the materials. In efficient modern MHP-based solar cells, the perovskite layer is typically sandwiched between an electron transport layer (ETL) and a hole transport layer (HTL) to funnel the generated charges to the respective electrodes. It is well established that the

use of appropriate charge transport layers (CTLs), which should ideally also be charge selective,<sup>[7–9]</sup> helps to suppress non-radiative recombination as well as to enhance the open-circuit voltage ( $V_{OC}$ ) and fill factor (FF).<sup>[7,8,10,11]</sup> Therefore, accessing and understanding the electronic properties of device-relevant interfaces of MHPs are of pivotal importance for knowledge-based device optimization.


In contrast to the well-understood impact of the interfacial electronic energy level alignment on the  $V_{OC}$  of organic<sup>[12–14]</sup> and conventional inorganic solar cells,<sup>[15,16]</sup> the relation between the energy levels at perovskite-based interfaces and the  $V_{OC}$  remains yet subject of debate. This can be partially ascribed to the diversity of perovskite samples employed in research, e.g., differences in composition,<sup>[17–19]</sup> stoichiometry,<sup>[20–22]</sup> and preparation environment,<sup>[23]</sup> which often results in quite different electronic behavior when forming interfaces with transport layers.<sup>[24,25]</sup> For instance, studies have shown that basic electronic characteristics, e.g., the apparent *n*- or *p*-type character, of MHP films can be controlled not only by the stoichiometry of the perovskite precursors<sup>[20,22]</sup> but also by the substrate work function ( $\Phi_{sub}$ )<sup>[23,26–28]</sup> and history of sample handling (e.g., air exposure),<sup>[23,27]</sup> which can lead to conflicting data interpretation if these variations are not taken into account. Light-induced band bending at the interface, of misaligned transport layers, was also

F. Zu, L. Frohloff, D. Shin, N. Koch  
Institut für Physik & IRIS Adlershof  
Humboldt-Universität zu Berlin  
12489 Berlin, Germany  
E-mail: norbert.koch@physik.hu-berlin.de

M. Roß, S. Albrecht, N. Koch  
Helmholtz-Zentrum Berlin für Materialien und Energie GmbH  
12489 Berlin, Germany

N. Tessler  
Sara and Moshe Zisapel Nanoelectronics Center  
Andrew & Erna Viterbi Department of Electrical and Computer  
Engineering  
Technion  
Haifa 32000, Israel

S. Albrecht  
Electrical Engineering and Computer Science  
Technical University Berlin  
10587 Berlin, Germany

 The ORCID identification number(s) for the author(s) of this article can be found under <https://doi.org/10.1002/solr.202101065>.

© 2022 The Authors. Solar RRL published by Wiley-VCH GmbH. This is an open access article under the terms of the Creative Commons Attribution License, which permits use, distribution and reproduction in any medium, provided the original work is properly cited.

DOI: 10.1002/solr.202101065

suggested as a source for mitigating the  $V_{OC}$  degradation.<sup>[29]</sup> In addition, the presence of surface band bending induced by surface states can further complicate the ready understanding of MHPs' intrinsic electronic properties<sup>[30]</sup> and tuning of their energy levels at junctions with transport layers.<sup>[31]</sup> Likewise of importance, the majority of reported energy level situations of MHPs and their interface, most frequently obtained from ultraviolet photoelectron spectroscopy (UPS) experiments, were probed in dark,<sup>[25,32,33]</sup> i.e., the electronic ground state, but this can substantially differ from that under visible light illumination.<sup>[31,34–36]</sup> The latter links directly to the device operation condition and deserves a thorough and systematic investigation. In recent work, it was shown that the energy levels of thin organic CTLs deposited on top of MHP films exhibit an unexpected photoexcitation-driven energy level realignment.<sup>[37]</sup> Thus, the ground state energy level alignment of perovskite-based interfaces can be very different from that under device operation. Hence, to further develop strategies to maximize device efficiency, it is of fundamental importance to obtain better insights into the energy level alignment mechanisms at MHP/CTL interfaces in dark and under illumination. For instance, it is hitherto unknown whether the energy level alignment at the buried interface between a CTL and a thick MHP film on top can also exhibit light-induced energy level shifts.

Here, we assess the energy level alignment of a modern double cation perovskite, in dark and under solar illumination, deposited onto various organic CTLs with charge-selective character. In contrast to the common conception that the energy level alignment is fixed once an interface is formed, using UPS measurements, we obtain strong indications that the energy levels of the double cation perovskite, when deposited on charge-selective transport layer substrates, shift rigidly and reversibly under visible light illumination compared to the dark state. This is concluded from light-induced parallel shifts of the MHP's surface electrostatic potential (SEP) (often referred to as work function ( $\Phi$ ) in the electronic ground state) and valence band (VB), yielding constant ionization energy (IE) values. In contrast, the perovskite's energy levels remain unaffected by illumination when a charge nonselective organic transport layer substrate is employed. The experimental observations can be understood by a mechanism, in which photogenerated charge carriers within the perovskite layer are efficiently separated at the interface to the charge-selective organic layer, resulting in the accumulation of excess electrons or holes within the perovskite under quasi-open-circuit conditions. As a result, the perovskite energy levels exhibit a realignment with respect to those of the CTL induced by free charge carrier accumulation, which leads to either upward or downward shifts, depending on whether an HTL or an ETL substrate is employed, respectively. The realignment results from an abrupt "interface dipole" due to charge accumulation on both sides of the CTL/perovskite interface, or an electrostatic shift of the perovskite levels due to redistribution of photogenerated charge carriers at the direct contact with the CTL layer on the length scale of a few unit cells, where the latter features a weak electronic coupling between the two materials. Light-induced photovoltage can be ruled out to play a role, as this would lead to energy level shifts in a direction opposite to that observed experimentally. The proposition that the energy levels of MHPs can realign with respect to those of a CTL underneath

under illumination stresses the importance of assessing interfacial energy levels also under device operation relevant conditions and not only in the electronic ground state. With this knowledge, improved understanding of device functionality and future improvements are enabled.

## 2. Results

### 2.1. Energy Level Realignment at HTL/Perovskite Interfaces

For an initial demonstration of the effect of visible-light-induced charge accumulation on the interfacial energy level alignment, we chose poly-[bis-(4-phenyl)-(2,4,6-trimethylphenyl)-amin] (PTAA) as HTL as it is widely used in efficient *p-i-n* perovskite solar cells.<sup>[10,38]</sup> First, the bare PTAA film deposited onto indium-tin-oxide (ITO) was investigated by UPS. The HTL exhibits an essentially constant  $\Phi$  of 4.37 eV and highest occupied molecular orbital (HOMO) level onset at 0.68 eV binding energy (with respect to Fermi level ( $E_F$ ) at 0 eV) when measured in dark and under illumination (white light with  $\approx 1.5$  sun intensity). The corresponding UPS spectra are shown in Figure S1 in the Supporting Information). To establish the band alignment at the PTAA/perovskite interface,  $\text{FA}_{0.85}\text{Cs}_{0.15}\text{PbI}_3$  films with different thicknesses ranging from  $\approx 3$  to  $\approx 580$  nm were vacuum-deposited onto PTAA/ITO substrates, and UPS measurements were performed for each perovskite thickness. In addition, secondary electron cutoff (SECO) measurements were acquired under varied UV fluxes (excitation of photoelectrons) by adjusting the monochromator, while the VB spectra were recorded at high UV flux to obtain an adequate signal-to-noise ratio. As shown in Figure 1a, with increasing the perovskite thickness, the  $\Phi$  probed at low UV flux ( $\text{UV}_L$ , attenuation by  $\approx 150$  times compared to high UV flux) increases gradually from 4.35 to 4.79 eV for 580 nm. Upon applying the high UV flux ( $\text{UV}_H$ ), a slight increase in perovskite  $\Phi$  by 0.08, 0.11, and 0.11 eV is noticed at layer thicknesses of 3, 5, and 10 nm, respectively. In contrast, the perovskite  $\Phi$  remained unchanged at a

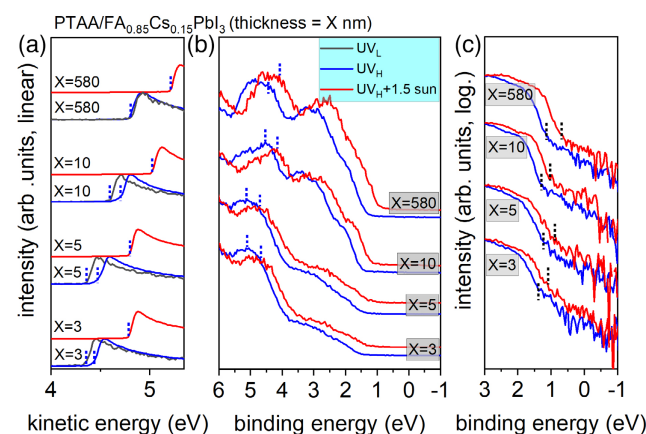


**Figure 1.** UPS spectra of ITO/PTAA/ $\text{FA}_{0.85}\text{Cs}_{0.15}\text{PbI}_3$  stacks with varied  $\text{FA}_{0.85}\text{Cs}_{0.15}\text{PbI}_3$  film thickness ranging from 3 to 580 nm. a) SECO; valence region on b) linear and c) logarithmic intensity scale.  $\text{UV}_L$  (gray lines) and  $\text{UV}_H$  (blue lines) denote the UV flux at low (attenuation by  $\approx 150$  times compared to high flux) and high intensity, respectively.

layer thickness of 580 nm upon varying the UV flux. Likewise, the valence spectra, displayed in Figure 1b,c, exhibit a rigid shift toward lower binding energy upon increasing the perovskite layer thickness. It is noted that the perovskite thickness of 3 nm, which corresponds to roughly 4 unit cells of the  $\text{PbI}_6$  lattice,<sup>[39]</sup> still retains the characteristic overall perovskite VB line shape, indicating the formation of intact perovskite. Taking into account the small UV-induced changes of  $\Phi$ , the VB onsets under low UV flux are then extracted at 1.48, 1.39, and 1.42 eV binding energy (with respect to  $E_F$  at 0 eV) for layer thicknesses of 3, 5, and 10 nm, respectively. With the material's bandgap of  $\approx 1.51$  eV,<sup>[40]</sup> the conduction band (CB) onsets at each layer thickness are retrieved. The key electronic parameters as determined from UPS are summarized in **Table 1**. The rigid changes in perovskite  $\Phi$  and VB as a function of layer thickness indicate band bending upon contact with PTAA. The energy level alignment at the PTAA/ $\text{FA}_{0.85}\text{Cs}_{0.15}\text{PbI}_3$  interface in dark, as shown in **Figure 2a**, thus corresponds to a type-II heterojunction with a large energy offset of  $\approx 0.80$  eV for hole extraction from the perovskite to the PTAA.

Illumination of the PTAA/ $\text{FA}_{0.85}\text{Cs}_{0.15}\text{PbI}_3$  stacks at each layer thickness with white light (intensity equivalent to 1.5 sun) during UPS measurements rigidly raises the sample SEP by  $\approx 0.43$  eV for all cases. Here, we use the term SEP under illumination to differentiate from  $\Phi$  measured under  $\text{UV}_L$ , which can be regarded as the ground state (dark condition); both are measured with respect to  $E_F$  of the conductive substrate. The shift of the SEP is quantitatively identical with the shift of the VB, as seen in Figure 1b,c, which lifts the perovskite VB onset toward the PTAA HOMO level onset. In addition, all energy levels recover to their initial values after switching off the light, as shown in Figure S2, Supporting Information, thus pointing to an electrostatic origin of these reversible shifts. Given that the energy levels

**Table 1.** Key electronic parameters determined from UPS measurements as a function of perovskite layer thickness and excitation by UV and visible light. The SEP in dark corresponds to the work function. VB onsets are extrapolated on a logarithmic intensity scale, to accurately infer the band edge position for perovskites.

		SEP [eV]	VB onset [eV]	CB onset [eV]
3 nm	$\text{UV}_L$	4.35	1.48 <sup>a)</sup>	0.03
	$\text{UV}_H$	4.43	1.40	/
	$\text{UV}_H + 1.5$ sun	4.78	1.06	0.45
5 nm	$\text{UV}_L$	4.36	1.39 <sup>a)</sup>	0.12
	$\text{UV}_H$	4.47	1.28	/
	$\text{UV}_H + 1.5$ sun	4.80	0.96	0.55
10 nm	$\text{UV}_L$	4.59	1.42 <sup>a)</sup>	0.09
	$\text{UV}_H$	4.70	1.31	/
	$\text{UV}_H + 1.5$ sun	5.02	1.00	0.51
580 nm	$\text{UV}_L$	4.79	1.14 <sup>a)</sup>	0.37
	$\text{UV}_H$	4.79	1.14	/
	$\text{UV}_H + 1.5$ sun	5.21	0.74	0.77

<sup>a)</sup>VB onsets under  $\text{UV}_L$  are estimated from the perovskite  $\Phi$  difference between  $\text{UV}_L$  and  $\text{UV}_H$ .  $\text{UV}_L$  and  $\text{UV}_H$  denote the low and high UV fluxes, respectively.

of PTAA did not shift upon light irradiation (see earlier discussion), the underlying mechanism is based on the photogeneration of carriers in the perovskite layer and subsequent hole transfer to the HTL, which results in electron accumulation within the perovskite layer. Because the light-induced level shift of the thin perovskite films (starting from 3 nm) is nearly identical to that of the 580 nm film, we conclude that most of the accumulated negative charge within the perovskite is located very close to the interface with PTAA. This is further corroborated by the fact that the high UV flux can already induce noticeable shifts at the PTAA/perovskite interface, whose effect becomes neglectable with perovskite thickness at 580 nm.

To facilitate deriving an interfacial energy level diagram, the same sample stack was modeled in a device simulation under illumination (see Table S1 and Figures S3–S5 in the Supporting Information). The main purpose of this was to obtain insight into a plausible charge density distribution within the sample. Two possible scenarios were modeled: 1) a constant energy level offset between PTAA and the perovskite (as observed from the UPS measurements in dark) and 2) with the perovskite VB onset shifted toward the HOMO onset of PTAA. The latter model is motivated by the reported photoinduced level realignment for organic CTLs deposited on top of a perovskite film, where even the levels of the organic layer directly touching the perovskite shifted.<sup>[37]</sup> In analogy, if the electronic coupling between the perovskite deposited on top of the organic layer is comparably weak, the electron accumulation within the perovskite could shift the perovskite energy levels upward until its VB maximum lines up with the HOMO level of PTAA. This is illustrated in the energy level diagram in Figure 2b. For the more conventional model, with the energy level offset at the contact of PTAA and the perovskite fixed, the energy level diagram under illumination is shown in Figure 2c. In both models, huge electron density accumulation within the perovskite layer close to the interface with PTAA is found, with almost flat band conditions throughout the thick film. In turn, positive charge accumulation within the PTAA layer at the interface is found in the simulations, generating an abrupt “interface dipole”-like situation. However, the density of positive charge accumulated in PTAA for the model shown in Figure 2b is vanishingly small, and would thus facilitate better hole extraction compared to the model of Figure 2c. Because it is not possible to assess the energy levels of PTAA buried underneath the perovskite directly in the experiment, we cannot formally rule out one of the two models at this point.

## 2.2. Energy Level Realignment at ETL/Perovskite Interfaces

To further demonstrate the effect of charge-selective transport layers on interfacial energy level (re-)alignment, the ETL material 1,4,5,8,9,12-hexa-azatriphenylhexacarbonitrile (HATCN) is employed. Because of its high electron affinity ( $>4.9$  eV<sup>[41]</sup>) and IE, energy offsets supporting electron extraction and hole blocking are expected at its interface with perovskite layers. Also here, the UPS results of bare HATCN/ITO substrate are mentioned first (data shown in Figure S6 in the Supporting Information). The energy levels of HATCN show constant positions independent of illumination. Next, the thick  $\text{FA}_{0.85}\text{Cs}_{0.15}\text{PbI}_3$  sample (580 nm) deposited on the HATCN/ITO substrate exhibits a  $\Phi$

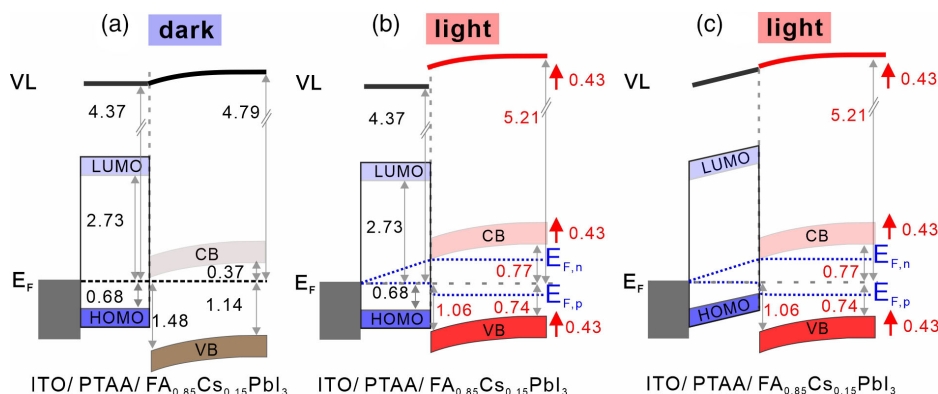


**Figure 2.** Schematic energy level diagrams of ITO/PTAA/FA<sub>0.85</sub>Cs<sub>0.15</sub>PbI<sub>3</sub> stack in a) dark and under b) and c) 1.5 sun white light irradiation intensity. b) Depicts the model where the energy levels of the perovskite are abruptly shifted with respect to those of PTAA and c) shows the model with fixed interfacial energy levels as determined for the dark situation. VL refers to the vacuum level. The indicated energy values are given with respect to  $E_F$  set to zero. The blue dashed lines in b) and c) represent the quasi Fermi levels  $E_{F,n}$  and  $E_{F,p}$  for electrons and holes, respectively; the red arrows and numbers indicate the illumination-induced change of the perovskite energy levels with respect to  $E_F$  of the conductive ITO substrate.

of 4.55 eV, despite the high HATCN/ITO  $\Phi$  of 5.09 eV. Such difference is likely caused by the formation of band bending at the HATCN/perovskite interface, as observed in the case of PTAA substrate. As shown in **Figure 3b,c**, the VB onset of the thick FA<sub>0.85</sub>Cs<sub>0.15</sub>PbI<sub>3</sub> is positioned at 1.19 eV binding energy, extrapolated on the logarithmic intensity scale. The HATCN/FA<sub>0.85</sub>Cs<sub>0.15</sub>PbI<sub>3</sub> interface thus exhibits a type-II heterojunction, however, with HATCN acting as an ETL layer with an energy offset for electron extraction, as seen from the schematic energy level diagram in **Figure 3d**.

In analogy to the HTL example mentioned earlier, UPS measurements were performed on this HATCN/FA<sub>0.85</sub>Cs<sub>0.15</sub>PbI<sub>3</sub> stack, which show clear downward shifts of perovskite energy levels by 0.11 eV upon illumination, i.e., the opposite direction observed with the HTL. This is observed in **Figure 3a** for the SECO and **Figure 3b,c** for the VB spectra, where the SEP (VL) decreases to 4.44 eV, accompanied by an equivalent shift of the VB onset by 0.11 eV toward higher binding energy. As a result, the CB minimum position of the perovskite is brought closer toward the lowest unoccupied molecular orbital level onset of HATCN, either by the light-induced “interface dipole” or by the energy level realignment, as discussed in detail earlier for the HTL case. The corresponding energy level diagram is displayed in **Figure 3e** for the realignment model, that for the “interface dipole” model in **Figure S7** in the Supporting Information. Upon illumination, the downward shift of the perovskite energy levels is driven by the accumulation of excess holes within the perovskite layer, and the electrons are efficiently extracted to the HATCN acting as ETL. We would like to mention that given the possible presence of large energy offset at the interface in dark, the less than expected light-induced shifts of perovskite energy levels are likely due to the interface states in the HATCN, which leads to the reduction of hole accumulation in the perovskite layer, as shown in **Figure S6**, Supporting information. It is worth noting that the described illumination-driven energy level realignment occurs instantly and reversibly within a timescale of a second, long before any photoinduced degradation or decomposition can take place,<sup>[30,42]</sup> thus supporting the electrostatic nature of the phenomenon.

### 2.3. Lack of Energy Level Realignment at Interfaces with a Conductive Substrate

Abovementioned results demonstrate the light-induced energy level realignment at buried interfaces of a perovskite deposited on charge-selective transport layers, where shifts in opposite directions of perovskite energy levels are observed between the employed HTL and ETL. This prompts us to expand our investigation on a perovskite interface with a charge nonselective substrate. In this case, the FA<sub>0.85</sub>Cs<sub>0.15</sub>PbI<sub>3</sub> film was deposited on poly(3,4-ethylenedioxythiophene):polystyrene sulfonate (PEDOT:PSS) conductive polymer substrates. The UPS spectra of the PEDOT:PSS/FA<sub>0.85</sub>Cs<sub>0.15</sub>PbI<sub>3</sub> sample are shown in **Figure S8**, Supporting Information, which exhibit initially a similar level alignment to those using charge-selective transport layers in dark, with an  $\Phi$  of 4.67 eV and the VB onset 1.06 eV below  $E_F$ . However, illumination does not result in changes of the energy levels at the PEDOT:PSS/FA<sub>0.85</sub>Cs<sub>0.15</sub>PbI<sub>3</sub> interface, i.e., the positions of the perovskite SEP/VL and VB are constant, as presented in **Figure S8a** and **S8b**, Supporting Information, respectively. The energy level diagram is illustrated in **Figure S8d**, Supporting Information, and both photogenerated electrons and holes are free to transfer across the interface. Consequently, the electron and hole density in the perovskite film remain balanced, leading to the constant interfacial level alignment.

## 3. Discussion

It is noted that the observed realignment of perovskite energy levels at the interface with charge-selective CTLs appears to mimic the surface photovoltage (SPV) effect, which originates from a redistribution of photogenerated charge carriers upon super-bandgap photoexcitation, i.e., light-induced flattening of ground state band bending that can exist in semiconductors. Although downward band bending by 0.34 eV is observed in the perovskite toward the interface with PTAA in the ground

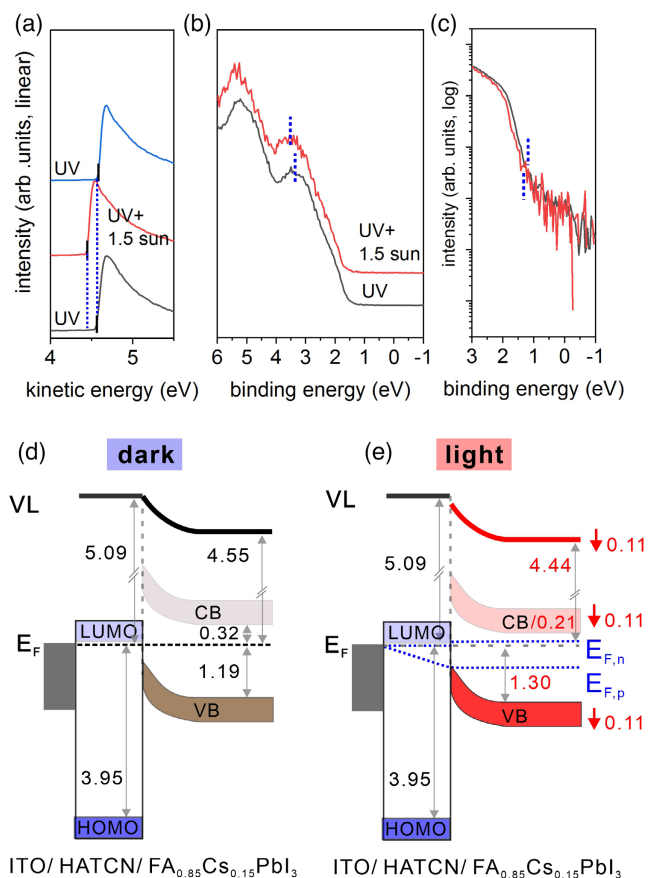


**Figure 3.** UPS spectra of the ITO/HATCN/FA<sub>0.85</sub>Cs<sub>0.15</sub>PbI<sub>3</sub> stack with perovskite thickness of 580 nm and energy level diagrams. a) SECO, VBs on b) linear and c) logarithmic intensity scale. Schematic energy level diagrams in d) dark and under e) 1.5 sun white light irradiation intensity. VL refers to the vacuum level. The indicated energy values are given with respect to  $E_F$  set to zero. The blue dashed lines in e) represent the quasi Fermi levels  $E_{F,n}$  and  $E_{F,p}$  for electrons and holes, respectively; the red arrows and numbers indicate the illumination-induced change of the perovskite energy levels with respect to  $E_F$  of the conductive ITO substrate. High UV flux was used for the UPS measurements as UV-induced energy shifts are neglectable for the thick perovskite sample. An upward band bending is assumed in perovskite layer toward the interface with HATCN in the ground state.

state (dark), SPV-induced shifts of the energy levels were not found to occur. Instead, the magnitude of band bending remains nearly the same at 0.32 eV under illumination, which can be seen from Figure 1 and Table 1. Therefore, band bending-induced photovoltage effects can be ruled out as a cause of the realignment of the perovskite energy levels upon illumination. In addition, we also note that all thick FA<sub>0.85</sub>Cs<sub>0.15</sub>PbI<sub>3</sub> films exhibit a rather pronounced n-type character, with  $E_F$  located close to the CB minimum, irrespective of  $\Phi$  of the substrate (covering a wide range of 4.37–5.09 eV), which is characteristic of a relatively high intrinsic (unintentional) n-doping level. In the case of mismatched work function of CTL and perovskite, interfacial ground state charge transfer between the CTL and the perovskite is expected to account for the development of a space-charge region, unless an unusually high density of states in the energy

gap of perovskites exists.<sup>[43]</sup> We do not observe indications for notable structured gap state density in the logarithmic intensity plots of the VB regions (Figures 1c and 3c), which has been observed by Zhang et al.<sup>[44]</sup> The slopes (or states) below the VB onsets seen in our perovskite spectra are likely linked to the tailing of VB states convoluted with the experimental broadening (Gaussian function) of the electron analyzer, which constitutes the background line of the photoemission spectra.

Similar conclusions can be made for the HATCN/perovskite interface, as shown in Figure 3, where an upward band bending is expected to occur in the perovskite layer toward the interface. Here, downward band bending in the perovskite layer is unlikely to occur, as it would further enlarge the abrupt change of the vacuum levels at the interface, in contrast to the principle of establishing electronic equilibrium.

The abovementioned results thus demonstrate a novel fundamental physical phenomenon, i.e., illumination-driven interfacial energy level realignment due to free charge carrier accumulation in the perovskite layer, strongly confined to the interface. Before, only space-charge accumulation in organic CTLs deposited on top of perovskites was known.<sup>[37]</sup> As for photovoltaic applications, such illumination-driven level realignment at perovskite-based interfaces must be considered and implemented in device-level modeling of device characteristics; otherwise, conclusions from simulation results can be misleading for further device design.

## 4. Conclusion

The presented results demonstrate that the interfacial energy levels of the double cation perovskite film are not fixed, but can undergo reversible realignment upon illumination when charge-selective transport layer substrates are employed. Such realignment is driven by the accumulation of one charge carrier type in the perovskite layer at the interface, which shifts its energy levels with respect to those of the CTLs (including the direct contact) or induces an abrupt “interface dipole.” This is further corroborated by using PEDOT:PSS as a non-charge-selective conductive substrate, where the interfacial energy levels remain unchanged upon light irradiation, thus confirming the electrostatic nature of the disclosed phenomenon. Hence, it can be anticipated that interfaces of semiconductors beyond the ones investigated here with type-II junction, i.e., interfaces with charge carrier-selective character, may exhibit similar energy level realignment behavior upon photoexcitation if sufficient photogenerated carrier density residing at the interfaces can be created. The abovementioned results underline the need to establish a general and reliable framework for photoemission measurement protocols for perovskite-based interfaces under illumination to unravel details of the working mechanism of pertinent devices.

## 5. Experimental Section

**Substrates:** ITO substrates (Automatic Research, Germany) were cleaned with acetone, DI water, and iso-propanol, by sonication for 10 min in each solution. After UV-ozone treatment for 10 min, the samples were transferred to a N<sub>2</sub>-filled glove box for PTAA deposition. The layer of

the PTAA (Sigma-Aldrich) with a thickness of 8 nm was spin-coated from a 2 mg mL<sup>-1</sup> toluene solution at 6000 rpm for 30 s. The films were annealed on a hotplate at 100 °C for 10 min before perovskite deposition. The PEDOT:PSS (AI4083) layer was spin-coated at 4000 rpm for 50 s in air, followed by annealing at 150 °C for 10 min in the glove box.

The HATCN (Novaled) films with a thickness of 8 nm were thermally evaporated at a base pressure of 2 × 10<sup>-6</sup> mbar.

**Perovskite Sample Preparation:** For the perovskite deposition, lead iodide (99.99%, trace metals basis) from TCI, formamidinium iodide (FAI) from Greatcell Solar Materials, and cesium iodide from abcr GmbH were used without previous purification. The perovskite layers were deposited with a CreaPhys “PEROVap” thermal evaporation system integrated into a glove box with an inert nitrogen atmosphere. The temperature of the inner shielding, surrounding all evaporation sources, was set to -25 °C for all processes. The system was evacuated to a base pressure of 2 × 10<sup>-6</sup> mbar before the sources were heated. To measure the evaporation rate of each precursor material, three independent quartz crystal microbalances were used. For all processes, the evaporation rate of each material was kept constant by automatically adjusting the source temperature. According to the rates determined by the quartz crystal microbalance of each material, a perovskite with a thickness of ≈580 nm and composition of FA<sub>0.85</sub>CS<sub>0.15</sub>PbI<sub>3</sub> was obtained. The rotation speed of the substrate holder (10 rpm) and the substrate temperature (60 °C) were held constant for the entire deposition time.

**Photoemission Measurements:** UPS was conducted using a monochromated helium discharge lamp (HIS 13 FOCUS GmbH, photon energy of 21.22 eV) in an ultrahigh vacuum system (base pressure of 1 × 10<sup>-9</sup> mbar). With the monochromator, the visible light was eliminated and UV flux was significantly reduced (attenuation by a factor of ≈100 as compared to that of a standard helium lamp). All spectra were recorded at room temperature and normal emission using a hemispherical electron analyzer (SPECS Phoibos 100). The illumination experiments were conducted using a white halogen lamp (Solux MR16 4700 K, 50 W, daylight rendering) during UPS measurements with an intensity of ≈150 mW cm<sup>-2</sup>. The SECO spectra were recorded with a negative bias of 10 V applied to the samples.

## Supporting Information

Supporting Information is available from the Wiley Online Library or from the author.

## Acknowledgements

This work was funded by the Deutsche Forschungsgemeinschaft (DFG, German Research Foundation, Project numbers: 182087777-SFB951 and 423749265-SPP2196 “SURPRISE”) and the Helmholtz International Research School HI-SCORE (HIRS-0008).

Open access funding enabled and organized by Projekt DEAL.

## Conflict of Interest

The authors declare no conflict of interest.

## Data Availability Statement

The data that support the findings of this study are available from the corresponding author upon reasonable request.

## Keywords

energy level alignment, interfaces, organic charge transport layers, perovskites, photoelectron spectroscopy

Received: December 17, 2021

Revised: January 28, 2022

Published online: February 17, 2022

- [1] J. H. Im, C. R. Lee, J. W. Lee, S. W. Park, N. G. Park, *Nanoscale* **2011**, *3*, 4088.
- [2] Z. K. Tan, R. S. Moghaddam, M. L. Lai, P. Docampo, R. Higler, F. Deschler, M. Price, A. Sadhanala, L. M. Pazos, D. Credgington, F. Hanusch, T. Bein, H. J. Snaith, R. H. Friend, *Nat. Nanotechnol.* **2014**, *9*, 687.
- [3] X. Hu, X. Zhang, L. Liang, J. Bao, S. Li, W. Yang, Y. Xie, *Adv. Funct. Mater.* **2014**, *24*, 7373.
- [4] A. Al-Ashouri, E. Köhnen, B. Li, A. Magomedov, H. Hempel, P. Caprioglio, J. A. Márquez, A. B. M. Vilches, E. Kasparavicius, J. A. Smith, N. Phung, D. Menzel, M. Grischek, L. Kegelmann, D. Skroblin, C. Gollwitzer, T. Malinauskas, M. Jošt, G. Matič, B. Rech, R. Schlatmann, M. Topič, L. Korte, A. Abate, B. Stannowski, D. Neher, M. Stollerfoht, T. Unold, V. Getautis, S. Albrecht, *Science* **2020**, *370*, 1300.
- [5] <https://www.nrel.gov/pv/cell-efficiency.html> (accessed: January 2022).
- [6] M. Stollerfoht, C. M. Wolff, Y. Amir, A. Paulke, L. Perdigón-Toro, P. Caprioglio, D. Neher, *Energy Environ. Sci.* **2017**, *10*, 1530.
- [7] Y. H. Lin, N. Sakai, P. Da, J. Wu, H. C. Sansom, A. J. Ramadan, S. Mahesh, J. Liu, R. D. J. Oliver, J. Lim, L. Aspitarte, K. Sharma, P. K. Madhu, A. B. Morales-Vilches, P. K. Nayak, S. Bai, F. Gao, C. R. M. Grovenor, M. B. Johnston, J. G. Labram, J. R. Durrant, J. M. Ball, B. Wenger, B. Stannowski, H. J. Snaith, *Science* **2020**, *369*, 96.
- [8] M. Stollerfoht, P. Caprioglio, C. M. Wolff, J. A. Márquez, J. Nordmann, S. Zhang, D. Rothhardt, U. Hörmann, Y. Amir, A. Redinger, L. Kegelmann, F. Zu, S. Albrecht, N. Koch, T. Kirchartz, M. Saliba, T. Unold, D. Neher, *Energy Environ. Sci.* **2019**, *12*, 2778.
- [9] S. Zhang, M. Stollerfoht, A. Armin, Q. Lin, F. Zu, J. Sobus, H. Jin, N. Koch, P. Meredith, P. L. Burn, D. Neher, *ACS Appl. Mater. Interfaces* **2018**, *10*, 21681.
- [10] M. Stollerfoht, C. M. Wolff, J. A. Márquez, S. Zhang, C. J. Hages, D. Rothhardt, S. Albrecht, P. L. Burn, P. Meredith, T. Unold, D. Neher, *Nat. Energy* **2018**, *3*, 847.
- [11] C. M. Wolff, F. Zu, A. Paulke, L. P. Toro, N. Koch, D. Neher, *Adv. Mater.* **2017**, *29*, 1700159.
- [12] A. Wilke, J. Endres, U. Hörmann, J. Niederhausen, R. Schlesinger, J. Frisch, P. Amsalem, J. Wagner, M. Gruber, A. Opitz, A. Vollmer, W. Brütting, A. Kahn, N. Koch, *Appl. Phys. Lett.* **2012**, *101*, 233301.
- [13] S. M. Menke, N. A. Ran, G. C. Bazan, R. H. Friend, *Joule* **2018**, *2*, 25.
- [14] N. K. Elumalai, A. Uddin, *Energy Environ. Sci.* **2016**, *9*, 391.
- [15] S. M. Sze, Y. Li, K. K. Ng, *Physics of Semiconductor Devices*, John Wiley & Sons, Inc, Hoboken, NJ **2007**.
- [16] W. Shockley, H. J. Queisser, *J. Appl. Phys.* **1961**, *32*, 510.
- [17] M. Saliba, T. Matsui, K. Domanski, J. Y. Seo, A. Ummadisingu, S. M. Zakeeruddin, J. P. Correa-Baena, W. R. Tress, A. Abate, A. Hagfeldt, M. Grätzel, *Science* **2016**, *354*, 206.
- [18] M. Saliba, T. Matsui, J. Y. Seo, K. Domanski, J. P. Correa-Baena, M. K. Nazeeruddin, S. M. Zakeeruddin, W. Tress, A. Abate, A. Hagfeldt, M. Grätzel, *Energy Environ. Sci.* **2016**, *9*, 1989.

- [19] P. Caprioglio, F. Zu, C. M. Wolff, J. A. Márquez Prieto, M. Stolterfoht, P. Becker, N. Koch, T. Unold, B. Rech, S. Albrecht, D. Neher, *Sustainable Energy Fuels* **2019**, *3*, 550.
- [20] Q. Wang, Y. Shao, H. Xie, L. Lyu, X. Liu, Y. Gao, J. Huang, *Appl. Phys. Lett.* **2014**, *105*, 163508.
- [21] J. Emara, T. Schnier, N. Pourdavoud, T. Riedl, K. Meerholz, S. Olthof, *Adv. Mater.* **2016**, *28*, 553.
- [22] P. Cui, D. Wei, J. Ji, H. Huang, E. Jia, S. Dou, T. Wang, W. Wang, M. Li, *Nat. Energy* **2019**, *4*, 150.
- [23] D. Shin, F. Zu, A. V. Cohen, Y. Yi, L. Kronik, N. Koch, *Adv. Mater.* **2021**, *33*, 2100211.
- [24] F. Zu, D. Shin, N. Koch, *Mater. Horizons* **2021**, *9*, 17.
- [25] S. Olthof, *APL Mater.* **2016**, *4*, 091502.
- [26] P. Schulz, L. L. Whittaker-Brooks, B. A. Macleod, D. C. Olson, Y. L. Loo, A. Kahn, *Adv. Mater. Interfaces* **2015**, *2*, 1400532.
- [27] D. Shin, F. Zu, N. Koch, *APL Mater.* **2021**, *9*, 081104.
- [28] S. Bitton, N. Tessler, *J. Mater. Chem. C* **2021**, *9*, 1888.
- [29] N. Tessler, Y. Vaynzof, *ACS Energy Lett.* **2020**, *5*, 1260.
- [30] F. S. Zu, P. Amsalem, I. Salzmann, R. Bin Wang, M. Ralaiarisoa, S. Kowarik, S. Duhm, N. Koch, *Adv. Opt. Mater.* **2017**, *5*, 1700139.
- [31] F. Zu, P. Amsalem, M. Ralaiarisoa, T. Schultz, R. Schlesinger, N. Koch, *ACS Appl. Mater. Interfaces* **2017**, *9*, 41546.
- [32] P. Schulz, E. Edri, S. Kirmayer, G. Hodes, D. Cahen, A. Kahn, *Energy Environ. Sci.* **2014**, *7*, 1377.
- [33] S. Wang, T. Sakurai, W. Wen, Y. Qi, *Adv. Mater. Interfaces* **2018**, *5*, 1800260.
- [34] F. Zu, C. M. Wolff, M. Ralaiarisoa, P. Amsalem, D. Neher, N. Koch, *ACS Appl. Mater. Interfaces* **2019**, *11*, 21578.
- [35] T. Hellmann, C. Das, T. Abzieher, J. A. Schwenzer, M. Wussler, R. Dachauer, U. W. Paetzold, W. Jaegermann, T. Mayer, *Adv. Energy Mater.* **2020**, *10*, 2002129.
- [36] B. N. Lee, S. Kirmayer, E. Edri, G. Hodes, D. Cahen, *J. Phys. Chem. Lett.* **2014**, *5*, 2408.
- [37] F. Zu, J. H. Warby, M. Stolterfoht, J. Li, D. Shin, E. Unger, N. Koch, *Phys. Rev. Lett.* **2021**, *127*, 246401.
- [38] F. Penã-Camargo, P. Caprioglio, F. Zu, E. Gutierrez-Partida, C. M. Wolff, K. Brinkmann, S. Albrecht, T. Riedl, N. Koch, D. Neher, M. Stolterfoht, *ACS Energy Lett.* **2020**, *5*, 2728.
- [39] A. Poglitsch, D. Weber, *J. Chem. Phys.* **1987**, *87*, 6373.
- [40] P. F. Ndione, Z. Li, K. Zhu, *J. Mater. Chem. C* **2016**, *4*, 7775.
- [41] H. Yoshida, K. Yoshizaki, *Org. Electron.* **2015**, *20*, 24.
- [42] F. Zu, T. Schultz, C. M. Wolff, D. Shin, L. Frohloff, D. Neher, P. Amsalem, N. Koch, *RSC Adv.* **2020**, *10*, 17534.
- [43] M. Oehzelt, N. Koch, G. Heimel, *Nat. Commun.* **2014**, *5*, 4174.
- [44] F. Zhang, J. C. Hamill, Y. L. Loo, A. Kahn, *Adv. Mater.* **2020**, *32*, 2003482.